Proceedings of ASME 2018 37th International Conference on Ocean, Offshore and Arctic Engineering
OMAE2018
June 17-22, 2018, Madrid, Spain

OMAE2018-78533

INVESTIGATION OF AN AIR-CUSHION SUPPORTED SOLAR ISLAND

Trygve Kristiansen
Dept. of Marine Technology
University of Science and Technology (NTNU)
Otto Nielsens v 10, 7091 Trondheim, Norway
Email: trygve.kristiansen@ntnu.no

Petter Borvik[1]
Dept. of Marine Technology
University of Science and Technology (NTNU)
Otto Nielsens v 10, 7091 Trondheim, Norway

ABSTRACT

A preliminary investigation of a low-weight carrying marine platform concept was conducted by means of experiments and approximate theories. The platform consists of a circular elastic tube with circular cross-section, covered with an air-supported membrane deck. A vertical skirt is added along the circumference of the model to avoid air-leakage. We refer to this concept as floating solar island. Solar islands have recently gained interest. The models were subjected to waves. Both regular and irregular wave tests were conducted. Tests with the absence of the membrane (floater only) were also conducted. The general behaviour and failure modes were investigated. Failure modes include over-topping with flooding as consequence, as well as out-of-water incidents and membrane wear with air leakage as consequence. A systematic variation of wave conditions revealed for which wave conditions flooding occured. Out-of-water incidents of the skirt were not observed. Vertical accelerations were measured at eight positions along the circumference of the model, and the heave, pitch and first flexible mode motions were re-constructed by modal theory. The modal responses were compared to theory based on linear potential flow assumption, both for the floater model only, and with simplified theory accounting for the air-cushion of the island in heave. The theory was able to predict the global behaviour reasonably well, although important discrepancies were observed. More detailed studies, involving experiments with more instrumentation and development of theory, must be conducted in case deeper understanding of this relatively complex, hydro-elastic concept is needed.

INTRODUCTION

In view of predicted global trends in energy consumption, achievement of established climate goals requires the installation by the year 2050 of 10 TW of carbon-neutral power, which can only be produced in a sustainable manner using solar energy [5]. Harvesting solar energy requires, however, large areas, and due to scarcity of suitable land area close to populated areas, making use of the sea close to shore could offer an interesting alternative. This has recently gained interest. One could also consider the possibility of harvesting solar energy in marginally exposed areas in the ocean in order to produce liquid fuel based on the CO2 in the ocean. For large scale harvesting, one would need to seek cost-efficient marine-based platforms, able to carry (low-weight) solar panels. Different concepts could be considered, depending on the environmental conditions. One possible concept is that considered in the present paper.

The main property of this concept is that the weight of the solar panels is carried by an air-cushion supported membrane. A slight over-pressure is induced in the air-pocket, depending on the weight per area of the equipment. The use of air-cushions to support marine and offshore structures is not a new idea. It is used, for instance by Surface Effect Vessels, (SES) [1]. The advantage is low resistance and good sea-keeping properties. A disadvantage is the so-called cobblestone effect, that is, resonance of the air-cushion due to the compressibility of air, which occurs at a frequency of about 2 Hz. [9] investigated still water resistance and sea-keeping properties of an air-supported MOB. He presented theory and numerical computations that supported the findings. Keeping a low draft was found essential for low still-

[1]Current affiliation: TechnipFMC, Lysaker 1366 Norway

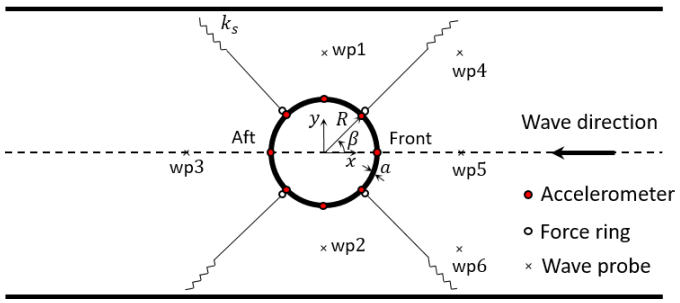

FIGURE 1. SCHEMATIC DESCRIPTION OF THE EXPERIMENTAL SET-UP.

water resistance. He confirmed good sea-keeping properties. [8] presented an alternative formulation to solve for problems with air-cushion, including wave scattering and radiation. [4] presented theory for cases where air-compressibility matters, i.e. when structures are sufficiently large such that acoustic waves of frequency in the relevant wave frequency range occurs.

Due to that the compressibility of air does not Froude scale, one must, in general, perform model tests in cavitation tanks, where the ambient air pressure is lowered. This was not done in the present tests. However, the relevant wave frequencies where lower than the resonance frequencies of the air-cushion.

An example where resonance of the air-cushion was important, but still useful model tests were made in a standard wave basin (without lowering the ambient air pressure) was a case where an offshore platforms was lifted above regions of shallow water when towed to site (Bernard Molin, personal communication 2017). Particular measures was taken in order to achieve the correct natural periods of the system; a tuned elastic membrane was added to the model.

The paper is presented as follows. After this introduction, the presently conducted experiments are described. A simplified theory for heave, inspired by models for SES, is presented in the following section. Results are then presented, where the general behaviour as well as failure modes are discussed.

EXPERIMENTS

We consider a model scale of 1:50, although the experiments were carried out as a preliminary investigation of the concept, and not targeted towards a real model.

Three different models were tested, referred to as elastic island model, stiff island model and elastic floater. The model test set-up is illustrated schematically in Figure 1. The wave tank has length 28m, width 2.5m and the water depth was 1.0m. The diameter of the models was $2R = 1.0$m.

TABLE 1. MAIN PROPERTIES OF THE FLOATERS.

	m (kg/m)	EI (Nm^2)	a (m)	R (m)
Elastic	0.402	0.46	0.016	1.0
Stiff	0.685	14.4	0.0135	1.0

TABLE 2. MAIN PROPERTIES OF THE MAIN COMPONENTS OF THE MODELS.

	Weight (kg)	Size (m)
Flexible floater	1.26	
Stiff floater	2.15	
Deck	0.143	
Skirt	0.039	0.07
Bottom weight (in air)	0.062	
"PV panels" (plastic rulers)	0.145	
8 acc-meters	0.240	

Instrumentation

All three models were equally moored and instrumented. Eight (near) vertical accelerometers were mounted around the circumference of the models, mounted on top of the floater, 45 degrees apart. Six wave gauges were used; three upstream, one on each side and one at the rear. The mooring lines were near horizontal, each with a spring with stiffness $k_s = 17$N/m and pretension $F_p \simeq 2.0$N. The force rings were mounted at the attachment point at the floater.

The different harmonics of the measured signals presented throughout this paper were extracted by first band-pass filtering the signal using a standard FFT based band-pass filter, and next taking the average of the amplitudes over a (near) steady part of the band-passed signal.

Models

The elastic floater was constructed by a standard 32mm diameter electric corrugated pipe used in houses. Due to the corrugations, duct tape was spun around in order to achieve a more smooth surface. The bending stiffness of the bare, corrugated pipe was $EI = 0.127$ Nm^2. The tape increased the bending stiffness to $EI = 0.46$ Nm^2.

The stiff floater was constructed by standard HDPE pipe used as domestic water pipes. The stiffness was approximately 30 times higher than the flexible floater. The main model properties are listed in Tables 1 and 2. The two floater stiffnesses would be representative for HDPE and steel floaters in full scale.

Both island models had the same type of horizontal membrane forming an air-filled cushion, and vertical skirt with bottom

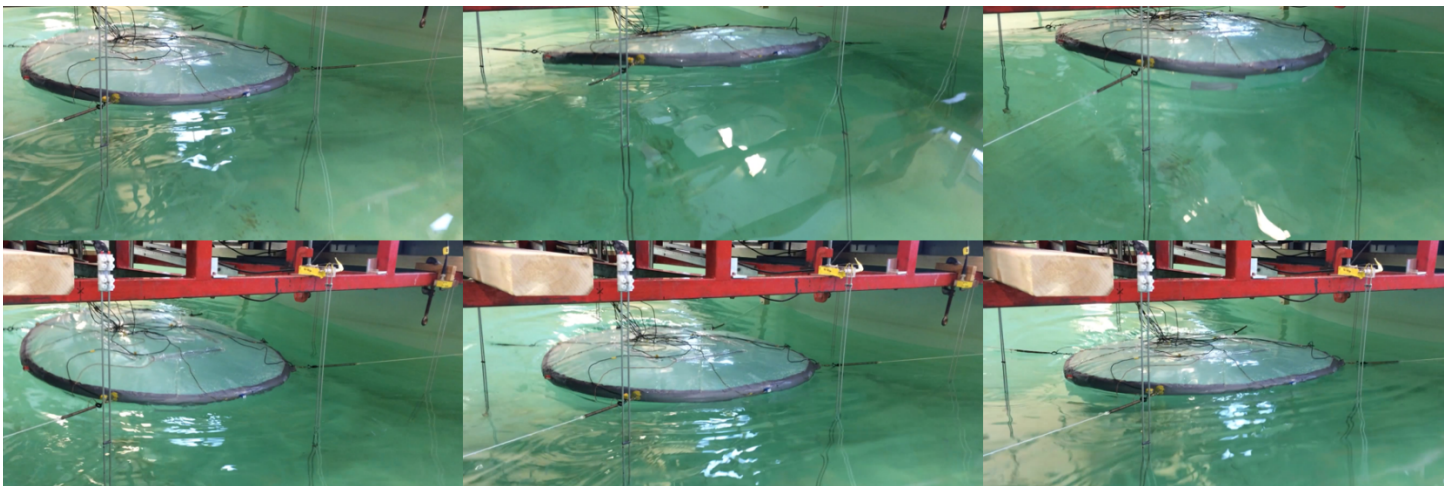

FIGURE 2. VIDEO SNAPSHOTS FROM REGULAR WAVE TEST WITH FLEXIBLE ISLAND MODEL. THE WAVE DIRECTION IS FROM RIGHT TO LEFT. WAVE PERIOD $T = 10$s. WAVE STEEPNESS $H/\lambda = 1/23$. HERE, THE FLOATER GOES OUT OF WATER, BUT THE SKIRT IS STILL PARTLY SUBMERGED.

weights. The membrane and skirt was made from 0.2mm thick plastic sheets as used as moist protection in floors of houses. They were flexible, but near inelastic. Plastic ruler elements were placed on top of the membrane to mimic the weight of the solar panels (approximately 30kg/m^2).

Air cushion

The over-pressure in the air-cushion was achieved by a compressor connected to the model by a thin, flexible hose. The hose was 5mm in diameter, and intruded the model via a sealed hole through the floater at the rear. The compressor scale was not adequately accurate to provide a controlled over-pressure, and the air-cushion pressure is therefore, unfortunately, not known. Instead, we estimated the over-pressure by observing the mean vertical set-up of the model (relative to no air-cushion), to be around 20Pa. This means that there was a 2mm water surface depression inside the model. Assuming a model scale of 1:50, this corresponds to 10cm full scale.

The air cushion had a clear destabilizing effect. This applied to both the elastic and stiff island models. For the elastic model, the flexibility of the floater allowed for significant local deformation, such that the floater would locally come out of water, revealing the upper parts of the skirt (statically). Six consecutive snapshots from video recordings of the flexible island model where this is illustrated are presented in Figure 2.

The rigid model would typically lean over to one side. This asymmetry with respect to the wave direction is revealed when comparing for instance the mooring loads at 45 and 315 degrees.

The (static) deformation varied between tests. Significant differences were observed between some of the repetition tests as a consequence.

The third model consisted of the *elastic floater* only; the same floater as used for the flexible island model, but without membrane and skirt. The elastic floater model is similar to the models used in studies of aquaculture farms in [3] and [7].

Wave conditions

Regular wave tests with wave periods corresponding to 4.2 - 11.2 seconds full scale were tested. The flexible model was tested in regular waves of four wave steepnesses; $H/\lambda = 1/58$, $1/46$, $1/35$ and $1/23$. Here, H represents the (linear) wave height, and λ the wave length. These tests were repeated five times. The other two models were tested in wave steepness $H/\lambda = 1/35$ only. These were repeated twice.

The amplitude of the first harmonic of the mean of the six wave signals are presented in Figure 3. Each symbol represents the mean value of the (first harmonic) amplitudes extracted from the six wave probes. The achieved wave amplitudes were in general within 3% of the theoretical values based on linear potential flow theory.

Some preliminary tests were also conducted with higher wave periods. However, flooding was observed for these, especially for the highest steepness. Due to the automatic test procedure applied, where long-duration tests including typically 100 - 200 regular wave conditions in one run is conducted. The long wave conditions were excluded to avoid water-on-deck which would disturb the non-flooded wave conditions considerably. Video snapshots illustrating flooding for $T = 12.1$s is provided later in the text (Figure 6).

Irregular wave conditions were also tested. For the elas-

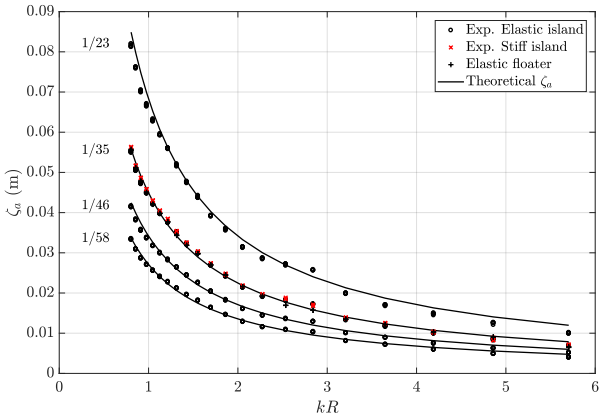

FIGURE 3. WAVE AMPLITUDES ACHIEVED IN THE TESTS (MODEL SCALE). EACH DATA POINT REPRESENT THE MEAN OF THE SIX WAVE GAUGES.

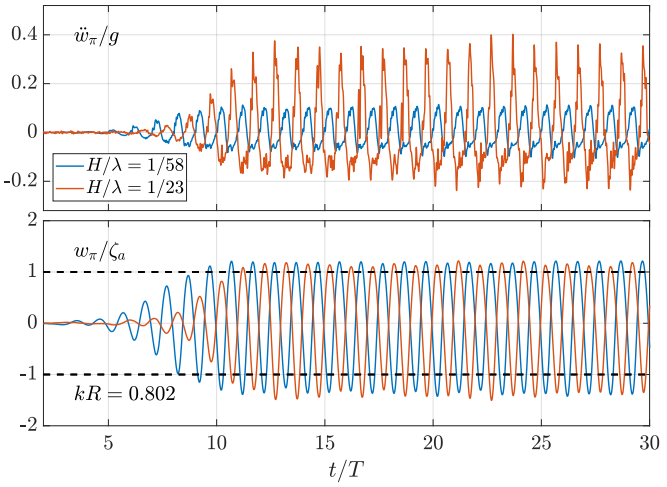

FIGURE 4. TIME-SERIES EXAMPLES FROM REGULAR WAVE TESTS WITH THE FLEXIBLE ISLAND. UPPER: ACCELERATION AT THE AFT ($\beta = \pi$). LOWER: VERTICAL MOTION BY INTEGRATION OF THE ACCELEROMETER SIGNAL AT THE AFT, NORMALIZED BY THE (MEASURED) INCIDENT WAVE AMPLITUDE ζ_a.

tic island model, a series of irregular waves with a systematic variation of H_s and fixed $T_p = 12$s was tested. The intended H_s were $1,2,..,8$m, while that achieved was $H_s =$ 0.93, 1.82, 2.70, 3.60, 4.43, 5.28, 6.17 and 7.00 m, based on an average of the six wave gauges.

Tests with combined regular waves and current were also conducted, but these are not reported here.

It is worth to mention that, although EI does not follow Froude scaling, but rather the scale to power four, the tests are representative in the sense of overall behaviour to other similar island diameters. Note that the compressibility of air does not neither follow Froude scaling. It is of importance to estimate the natural frequency of the air-cushion.

Pluck tests

Natural frequencies of the island models were briefly investigated by mounting four accelerometers on top of the membrane, giving the membrane a gentle pluck. Several resonance peaks were revealed. For the flexible island, the lowest peak occured at 5.2Hz. For the stiff island, the corresponding was 6.3Hz. We believe this to be due to resonant modes of the models itself (membrane and floater).

Theoretical estimates of the natural period in heave due to uniform compression of the air-cushion is 137Hz. The estimate is based on (4) by setting the excitation to zero and assuming the heave motion to be proportional to $e^{i\omega t}$.

A theoretical approximate estimate of the first mode horizontal standing acoustic wave inside the air-cushion is $c/2D =$ 167Hz, where $c = 334$m/s is the sound speed in air. The air-cushion has been approximated to be rectangular shaped. Note that in full scale (1:50), the latter would correspond to 3.3Hz.

Short discussion on error sources

The accelerometers and force rings went in-and-out of water during the experiments. This represents an error source, since the calibration factor reacts to temperature variations. We have not been able to quantify this source of error.

Due to that the air-cushion caused (non-repetitive) static and dynamic deformations of the flexible island model, the accelerometers were not entirely vertical. By visual inspection, the inclination angle was estimated to be up to 15-20 degress in some cases. Some effect of the acceleration of gravity was thus present. However, due to "cosine-effect", the influence on the results to be described here is not significant.

For the island models, there were some differences between the waves measured at the six different gauges (up to about 15% for some wave periods), indicating that the model caused some wave scattering. This applies to $kR \gtrsim 2.5$, where $k = 2\pi/\lambda$ is the wave number. In these cases, there are tank wall effects. Since diffraction is not taken into account, the wall effects were not attempted modelled.

Time-series examples

Time-series examples from regular wave tests of the flexible island model are provided in Figure 4. The acceleration at

the aft accelerometer, denoted $\ddot{w}_\pi$, non-dimensionalized by the acceleration of gravity, g, is given in the upper figure. Despite reasonably limitied wave steepnesses, the accelerations are far from sinusoidal. Significant higher harmonic content is present. In the lower figure, the vertical motion non-dimensionalized by the incident wave amplitude, ζ_a, is presented. The motions are deduced by integrating the presented acceleration signals twice in time. The motions are clearly more harmonic, as expected.

THEORY

We compare the experimental results with linearized potential flow theory combined with an Euler beam type of structural model for the floater, as presented in [6], and further developed by [7]. We first present the main elements of this theory. Next, we propose a method to include the effect of the air-cushion on heave in a simplified manner.

Floater motions

We use the zero-frequency limit of the linear potential flow theory for slender torus by [6], but include also an important term for pitch, which was introduced in [7].

The vertical motion $w(\beta,t)$ of the floater is decomposed in Fourier modes, symmetric about the x-axis,

$$w(\beta,t) = \sum_{n=0}^{\infty} b_n(t)\cos n\beta. \tag{1}$$

Heave is given by $\eta_3 = b_0$, pitch by $\eta_5 = b_1/R$ and flexible modes are represented by $b_{n\geq 2}$. The equation of motion is described by the beam equation provided in [7],

$$m\frac{\partial^2 w}{\partial t^2} + EI\frac{\partial^4 w}{\partial s^4} + \frac{EI}{R^2}\frac{\partial^2 w}{\partial s^2} = f_z(s,t), \tag{2}$$

where m is the floater mass per unit length, EI the structural bending stiffness, and $s = R\beta$ is the coordinate along the floater such that $\partial/\partial s = R^{-1}\partial/\partial\beta$. f_z is the vertical forces per unit length of the floater, and include wave excitation forces, added mass and damping forces, hydrodynamic restoring forces, and other external forces such as that from a net cage in case of an aquaculture farm (cf. for instance [3]), moorings and other point loads. The first two terms on the left hand side represent the standard Euler beam equation for a straight beam. The last term on the left hand side is introduced due to that the floater is a "circular beam"; the term is necessary in order to obtain correct pitch behaviour (i.e. that pitch is independent of EI).

As done in [6], we insert (1) into (2), multiply by $\cos m\beta$ and integrate over β from 0 to 2π. We exploit orthogonality of cosines, and obtain

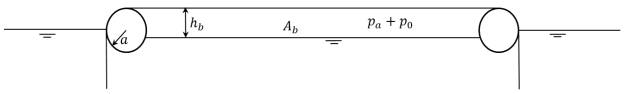

FIGURE 5. SIDE VIEW SKETCH OF SOLAR ISLAND, WITH PARAMETERS USED IN THE SIMPLIFIED AIR-CUSHION APPROACH.

$$(m + a_{33}^{(n)})\frac{\partial^2 b_n}{\partial t^2} + \left(\frac{EI}{R^4}\left(n^4 - n^2\right) + 2\rho g a\right) b_n = f_z^{\text{gen}}. \tag{3}$$

This is the zero-frequency limit of Eqn (21) in [6], except that the term proportional to n^2 was not included there. For the wave frequencies considered in the present study, there are minor effects of accounting for finite wave frequency in the theory. $a_{33}^{(n)}$ is the added mass per unit length for mode n. f_z^{gen} is the generalized vertical load per unit length. In the present work, only the wave excitation loads are included, where main components involve Bessel functions; cf. [6] for further details.

Air cushion effect on heave

We propose a simplified way of accounting for the presence of the air cushion for the heave motions, similar to what is done for Surface Effect Ships, cf. [1] (see pp. 151-154 therein). Here, the Froude-Kriloff type of vertical force from the waves are accounted for in a simplified manner. The method accounts for compressibility of air.

In the present wave conditions, wave frequencies considered are in general considerably lower than the resonance frequency of the air-cushion, and the simplified method is expected to represent the physics reasonably well. The air pressure is uniformly distributed inside the cushion.

For heave, the beam equation (2) is integrated along the circumference of the floater, and the resulting integrated equation is added to that of the air cushion. The result is

$$\left(2\pi R\left(m + a_{33}^{(0)}\right) + M_s\right)\frac{\partial^2 \eta_3}{\partial t^2} + \left(4\rho\pi R g a + \frac{A_b\gamma(p_0 + p_a)}{h_b}\right)\eta_3$$
$$= \left(\frac{\gamma p_0}{h_b} i\zeta_a q + 2\pi R\left(2\rho g a - \omega^2 a_{33}^{(0)}\right)\zeta_a J_0(\nu R)\right)e^{i\omega t}. \tag{4}$$

Here, ζ_a is the (linear) incident wave amplitude, M_s is the mass of the model excluding the floater, p_0 is the static over-pressure in the air-cushion, $\gamma = 1.4$ is the specific heat for air, J_0 is the Bessel function of the first kind, $\nu = \omega^2/g$ where $\omega = 2\pi/T$

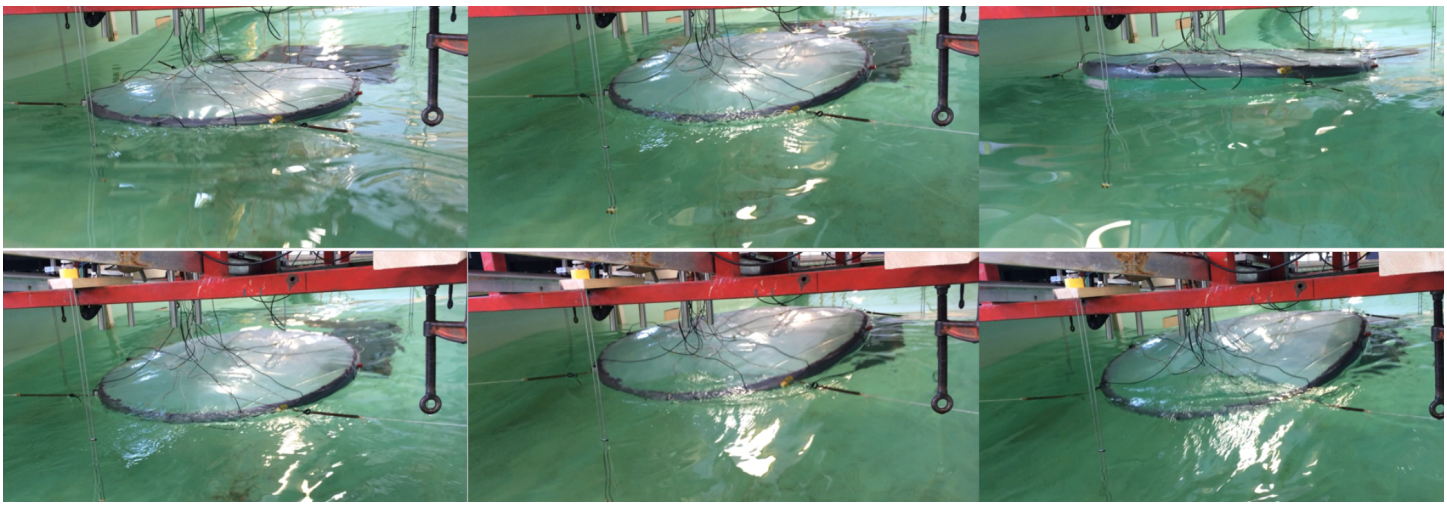

FIGURE 6. VIDEO SNAPSHOTS FROM REGULAR WAVE TESTS WITH THE FLEXIBLE ISLAND MODEL. WAVE DIRECTION TOWARDS THE CAMERA. REAR VIEW. $T = 12.1$s, $H/\lambda = 1/23$. NOTE FLOODED REAR PART IN THE TWO LOWER RIGHT PHOTOS.

is the circular wave frequency, q represents the (Froude-Kriloff) wave excitation on the air-cushion as given by

$$q = \int_0^{2\pi} \int_0^R \mathrm{e}^{ivr\cos\beta}\, r\,\mathrm{d}r\,\mathrm{d}\beta, \tag{5}$$

and the remaining parameters are described in Figure 5: $A_b = \pi R^2$ is the water-air interface enclosing the air-cushion from below, h_b is an averaged height of the air-cushion, neglecting the fact that the air-cushion has a small, negative curvature. We have neglected any elastic deformation of the membrane, and modelled it as a rigid wall. With a high over-pressure, the membrane is pre-tensioned sufficiently for this to be a reasonable assumption.

RESULTS

Selected results from the experiments are presented and discussed in view of the theory. We first briefly discuss failure modes, and show an illustrative example of flooding. Next, we present RAOs of the first three vertical modes, mooring loads, and higher harmonics of accelarations from regular waves. Next, a discussion of the irregular wave tests is provided.

Failure modes

Three examples of failure modes are flooding with water-on-deck as consequence, skirt out-of-water with massive air-leakage as consequence and membrane damages. The latter will lead to leakage which must be compensated for by a continuous power supply. Wear and tear will eventually result in holes in the membrane. The leakage rate and corresponding power needed to keep the over-pressure, can be estimated by an orifice flow analysis given the hole sizes and over-pressure. This was not investigated here.

The skirt was not observed to go entirely out of water in these tests, although it was observed to be nearly out of water in some tests with the regular waves of highest wave steepness $H/\lambda = 1/23$. The top right video snapshot in Figure 6 illustrates this. The photos are taken from the rear of the model.

Flooding was experienced. The two island models (both flexible and stiff) were both flooded for $H/\lambda = 1/23$ and wave periods $T \geq 12$s in preliminary regular wave tests. For this reason, waves with period higher than 11.2s were not included in the main, automated tests. The wave height was $H = 9.9$m. For the irregular waves with $T_p = 12$s and systematically increasing significant wave height, H_s, the models were flooded in the test with $H_s = 5.28$m. The maximum wave height during the 3 hour duration storm would be $H_{\max} \simeq 1.9 H_s = 10.1$m, which is consistent with the wave height of 9.9m in the regular wave test.

The vertical motions of the floater are considered in the following.

Vertical floater motion RAOs

Response amplitude operators (RAO) for the two vertical rigid-body modes (heave and pitch), and the first vertical flexible mode are presented in Figures 7 - 9. The body modes of motions were obtained by a standard modal analysis of the eight measured acceleration signals. Double time-integration based on FFT was in turn applied to obtain motions from accelerations. Since there

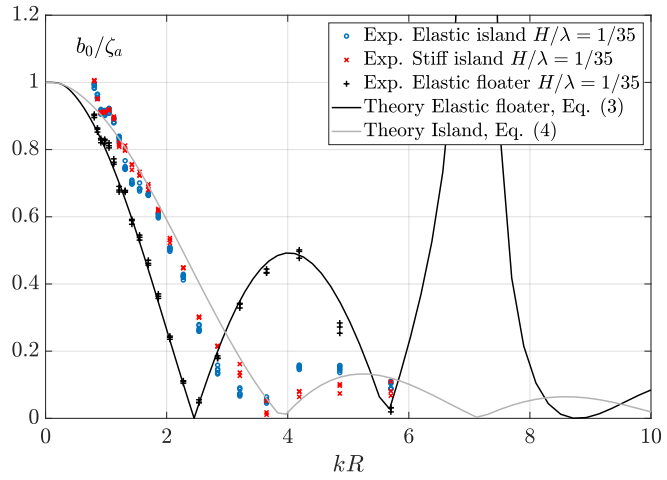

FIGURE 7. HEAVE RAO FROM REGULAR WAVE TESTS WITH $H/\lambda = 1/35$.

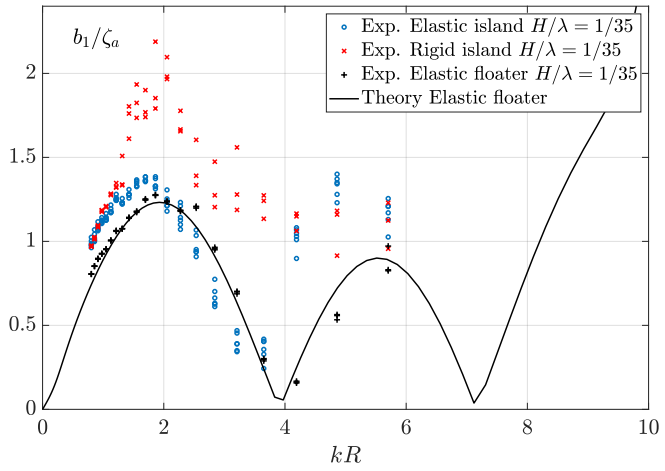

FIGURE 8. PITCH RAO FROM REGULAR WAVE TESTS WITH $H/\lambda = 1/35$. PITCH IS GIVEN BY $\eta_5 = a_1/R$.

were more accelerometers than number of modes predicted, a least-squares fit was applied.

Heave RAO. The heave RAOs are presented in Figure 7. For the elastic floater model, the experimental and theoretical RAOs, represented by black curve and symbols, are in general in good agreement. Similar good agreement for heave RAO of an elastic floater was presented by [7]. It is worth noting that the heave motions are water-plane stiffness dominated in the majority of the considered wave frequency range.

As far as the two island model goes, there are two main differences in the heave motions relative to that of the elastic floater model. One difference is that the RAOs are shifted towards right. The second is that they are considerably lower at the highest wave frequencies. Both these characteristics are captured to a reasonable extent by the simplified theory (4), although there are discrepancies, in particular for the flexible island model.

Pitch RAO. The pitch RAOs are presented in Figure 8. There are notable differences between the stiff and elastic islands; the former has considerably larger pitch motions. At $kR \simeq 2$, the pitch motions of the stiff island is almost a factor two higher than that of the flexible island. The elastic island model has similar pitch motions as the floater only model, except for a shift towards left. We did not attempt to investigate the effect of the membrane deck on pitch theoretically, as we did for heave.

It is worth noticing that for high wave periods (small kR) the pitch motions of the islands are larger than that of the floater model. This has relevance to flooding.

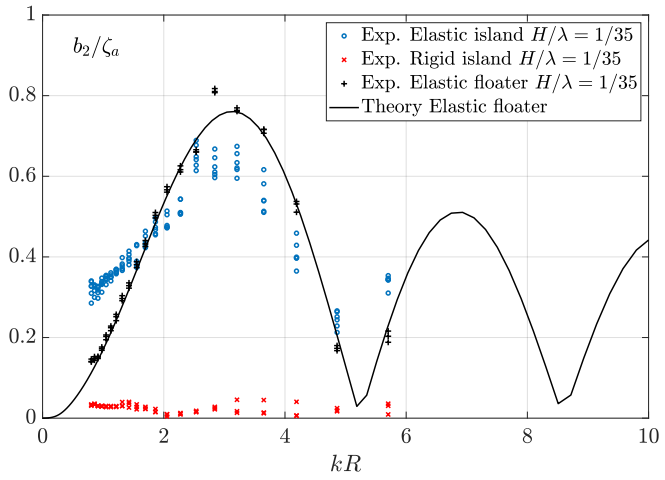

FIGURE 9. FIRST FLEXIBLE MODE RAO FROM REGULAR WAVE TESTS WITH $H/\lambda = 1/35$.

First flexible mode RAO. The first flexible mode RAOs are presented in Figure 9. As expected, the stiff model undergoes only minor flexible motions. The flexible island has some similarities to the flexible floater model, with a main difference that the flexible motions are significantly larger for long waves. For the longest regular wave tested ($kR = 0.802$), the first flex-

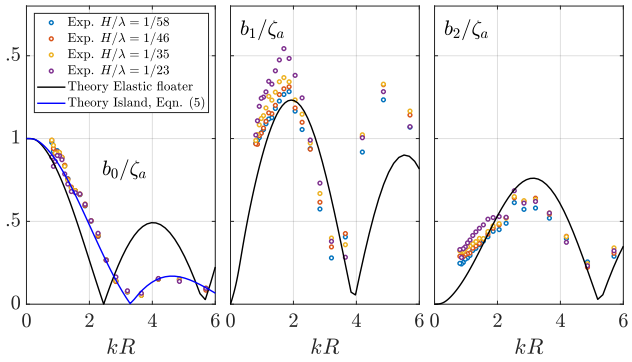

FIGURE 10. FLEXIBLE ISLAND RAO IN THE FIRST THREE MODES FOR ALL FOUR TESTED WAVE STEEPNESSES. EACH MARKER REPRESENTS THE AVERAGE OF SIX REPETITION TESTS.

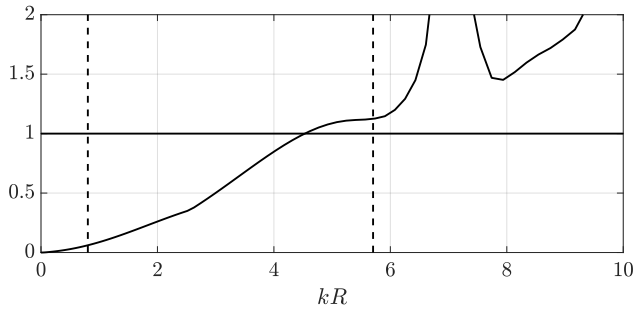

FIGURE 11. NON-DIMENSIONAL RELATIVE WAVE $\zeta_{\text{rel}}/\zeta_a = (\zeta - w)/\zeta_a$ ACCORDING TO THE THEORY (2). VERTICAL DASHED CURVES INDICATE THE TESTED RANGE OF REGULAR WAVES.

ible mode motion is more than twice that of the elastic floater model, and the trend indicates that the ratio will increase for longer waves.

Wave steepness dependence of the RAOs. Another observation is that there is a non-negligible dependence on wave steepness on the pitch and first flexible mode RAOs. This is illustrated in Figure 10. It is obvious that this has an effect on floater motions relative to the free-surface elevation, and therefore possible flooding. The reason for this amplitude dependence is not fully understood. A candidate is that the water-plane stiffness is sensitive to the relative motions due to the low draft and curved, circular cross-sectional shape, and therefore appreciably affected by non-linear effects in the basic harmonic ω.

Relative motions

We define the relative motion at any point along the circumference of the model by $\zeta_{\text{rel}} = \zeta - w$, where ζ represent the incident (linear) wave, and w the vertical motions (1). The relative wave for the elastic floater model can be easily deduced from the theory [7]. The maximum relative wave along the presently tested elastic floater model is presented in Figure 11. 20 modes vere sufficient for convergence.

The dashed, vertical curves indicate the range of the tested regular wave conditions. For the longest waves tested, there is almost no relative wave according to the theory; the floater more or less follows the waves. Still, the two *island models* experienced flooding at the rear.

From visual observations, there were significant local, vertical deformations at the rear of the elastic island model. The first flexible mode RAO in Figure 9 indicates that the island model exhibits significantly more flexible motions than the floater model at long waves. However, the first flexible mode is not adequate; a high number of modes would be needed in order to represent the visually observed behaviour.

A corresponding dense instrumentation would be needed to capture the behaviour experimentally. Due to the non-negligible weight of the accelerometers (cf. Table 2), rather than increasing the number of accelerometers, a better option would be to use an optical measurement system, or a network of strain gauges, in future studies.

The membrane needs to be modelled in future studies, since it introduces a possibly important structural coupling to the floater in the flexible modes. In the simple model for heave (4), the membrane was modelled as a rigid roof.

Nonlinear diffraction is also a contributing factor to flooding, although its role has not been investigated here. It is known that local, nonlinear diffraction occurs for a floater with circular cross-section [2]. The nonlinearity in the incident waves may matter.

The time-series of the vertical motion at the rear of the flexible island for the longest tested wave period provided in Figure 4 shows that the vertical motions are slightly larger than the (linear) incident wave amplitude ζ_a. The freeboard, which is the cross-sectional radius of the floater a, is more likely exceeded for the largest wave steepness.

Local rear, elastic deformation does not explain the flooding of the stiff island model. This model was also flooded at the rear for long and steep waves. This would need further studies. An elastic floater would in our minds be a much preferred due to its ability to follow the waves.

Mooring loads

The amplitude of the basic harmonic of the mooring loads for the three different models are presented in Figure 12. The loads are non-dimensionalized by $M_t g$, where M_t is the total

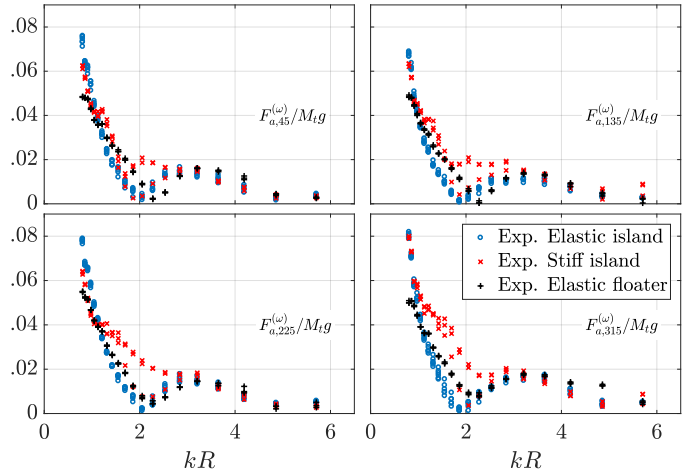

FIGURE 12. AMPLITUDES OF THE FIRST HARMONIC OF THE LOADS OF THE FOUR HORIZONTAL MOORING LINES. $H/\lambda = 1/35$.

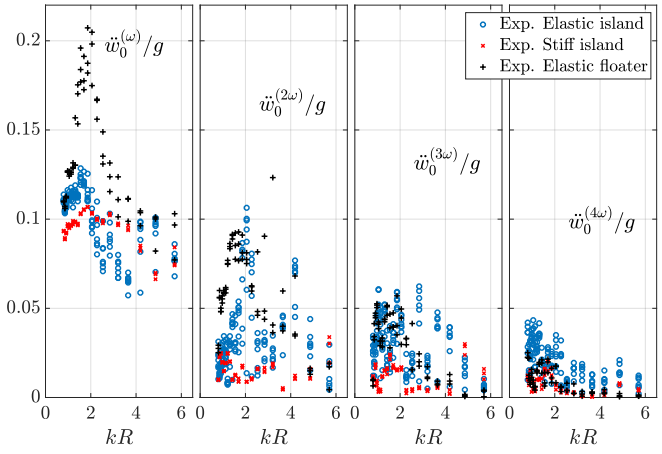

FIGURE 13. AMPLITUDES OF THE FIRST FOUR HARMONICS OF THE FRONT ACCELEROMETER ($\beta = 0$). $H/\lambda = 1/35$.

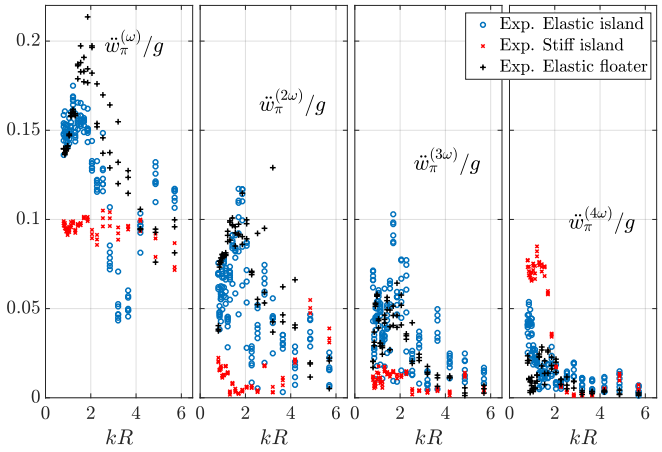

FIGURE 14. AMPLITUDES OF THE FIRST FOUR HARMONICS OF THE AFT ACCELEROMETER ($\beta = \pi$). $H/\lambda = 1/35$.

structural weight of the model, including the accelerometers. The wave steepness is $H/\lambda = 1/35$.

There is a distinct cancellation period at $kR \simeq 1.9$ for the flexible island, while $kR \simeq 2.2$ for floater only model. This corresponds to wave length-to-diameter ratios λ/D of 1.43 and 1.65, which is consistent with mooring loads in tests of aquaculture farms reported by [3].

The wave excitation and added mass loads due to the skirt are candidates for the differences.

We made an attempt to predict the mooring loads for the flexible island by a simple equation of motion in surge, accounting for the skirt in a simplistic manner, but we did not find the results to be satisfactory, so they are not presented here.

For the stiff island, the results from one of the three repetitions deviate from the other two; in one of them, the loads are very similar to those of the flexible island, in particular around the cancellation period, while in the other two repetitions, the loads show different trends. A main candidate to explain this seemingly random behaviour is the different static configuration due to the (statically) destabilizing effect of the air-cushion.

Acceleration - higher harmonics

As was demonstrated in the time-series presented in Figure 4, there were notable higher harmonics in the accelerations. High-frequency accelerations will matter for the equipment on the deck. Acceleration on the membrane deck itself was not measured in the present tests. One should then keep in mind the important scale effects of the air-cushion.

In Figures 13 and 14 the first four harmonics of the acceleration as measured at the front and aft of the models in regular wave tests are presented. The values are normalized with the acceleration of gravity, g. The results are not easily categorized, but it is worth to note that, for the two island models, the accelerations are in general higher in the aft than in the front, whereas in the case of the elastic floater model, they are much more similar.

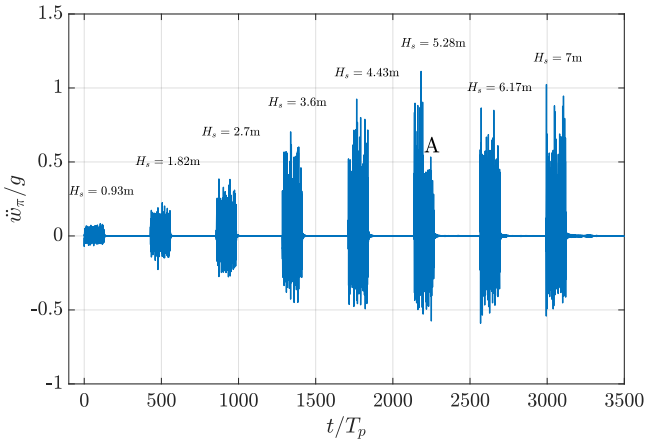

FIGURE 15. TIME-SERIES FROM IRREGULAR TESTS WITH $T_p = 12$s AND EIGHT DIFFERENT H_s. AFT ACCELEROMETER ($\beta = \pi$). FLEXIBLE SOLAR ISLAND. FLOODING OCCURED AT TIME MARKED BY "A".

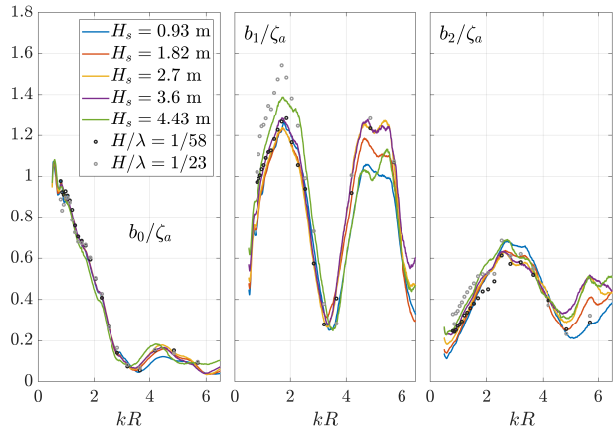

FIGURE 16. RAO FOR THE FIRST THREE MODES FROM THE IRREGULAR WAVE TESTS. FLEXIBLE SOLAR ISLAND.

The appreciable levels of higher harmonics of the acceleration is consistent with the findings of [7].

Irregular wave conditions

The time-series of the aft accelerometer as measured throughout the whole irregular wave test with eight significant wave heights, is provided in Figure 15. The time of flooding is marked by "A" in the figure. Significantly lower maximum accelerations are observed after flooding. The flooded water caused the membrane deck to get directly in contact with the underneath water surface, and considerable amount of water-on-deck.

RAOs for the first three vertical modes as obtained from the irregular wave tests without water-on-deck are presented in Figure 16. The time-series of each mode was, as in the regular wave cases, obtained by a standard modal analysis. Their Fourier transforms were smoothed by a standard built-in function in Matlab referred to as Savitzky-Golay filtering (with order 3 and frame length of 501). The six wave probe signals were filtered in the same manner, and the average of these was used to establish the RAOs.

The RAOs from the regular wave tests with the lowest and highest wave steepness are included for reference. The irregular and regular wave results are in general consistent with each other. For instance, the pitch and flexible mode RAO increase with increasing wave steepness. There are also differences. There is a more clear amplitude-dependence in the regular wave tests. The reason is that the amplitude-dependence differs throughout the irregular wave tests.

There are strengths and weaknesses with both irregular and

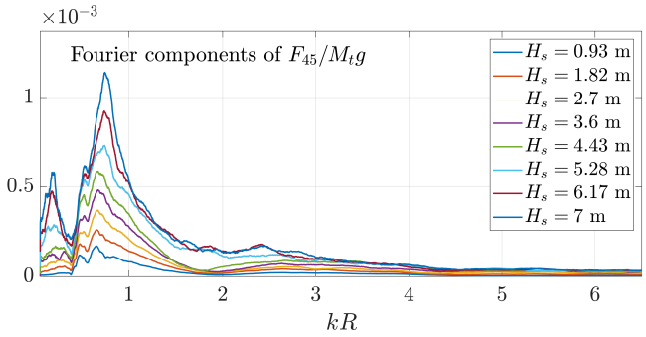

FIGURE 17. NORMALIZED FFT COMPONENTS OF FORCE IN MOORING LINE AT 45 deg FROM IRREGULAR TESTS WITH $T_p = 12$s AND VARYING H_s. FLEXIBLE SOLAR ISLAND.

regular wave tests. A particularly useful strength of regular wave tests is that one can isolate different effects. A pure irregular wave study would not reveal the important wave steepness dependence on the RAOs. Obtaining an RAO is quick in terms of laboratory time with an irregular test. However, with the automated testing procedure applied here, 200 - 300 regular wave tests are readily performed within one day, with a minimum of manual labour.

Normalized Fourier components of the mooring line at 45 deg are presented in Figure 17. The peak at $kR \simeq 0.2$ corresponds to the natural period in sway (4.7s in model scale). The peaks are more distinct in the cases with water-on-deck. A plausible reason is that the water-on-deck causes an increased critical damping. A major contributor to horizontal damping is that due to flow

separation at the lower ends of the skirt.

The irregularity around $kR \simeq 0.5 - 0.7$ is due to wave reflections from the beach; the beach has been shown to cause reflections in the order of 10% for waves that are of the order of three quarter of the beach length and longer.

CONCLUSIONS

Dedicated experiments of a solar island concept with an air-cushion supported, circular deck were conducted as part of a preliminary study. Tests with both flexible and stiff islands, as well as floater only models were carried out. Regular and irregular wave tests were conducted.

Simplified theoretical models based on linearized potential flow theory were presented for the vertical motions. A modal approach was taken. Heave, pitch and the first flexible mode were studied. Satisfactory comparison with the experiments was in general demonstrated, but important discrepancies were pointed out and discussed, with particular reference to flooding of the islands. Flooding was experienced for long and steep wave conditions; for regular waves with period 12.1s and wave steepness $H/\lambda = 1/23$, and consistently, for irregular waves with peak period $T_p = 12$s and $H_s = 5.28$m.

Mooring loads and higher harmonics of accelerations were also presented. Significant amplitudes of higher harmonics of the vertical accelerations were demonstrated for all models, relevant for loads on the installed solar panel equipment.

The experiments served well as a preliminary investigation. More instrumentation is needed in case one wants to obtain increased understanding of the structure's flexible responses.

Air leakage due to that the skirt went out of water was not observed, although nearly. Wear and tear with air leakage was not investigated, but is believed to be a major practical obstacle for the present concept, since a significant amount of power would be needed to keep the over-pressure in the air-cushion.

Due to possibility of flooding and the inevitable wear and tear of the membrane, we do not foresee the present concept as a feasible concept at exposed sites. However, at rather sheltered areas, it may offer an alternative as a cost-efficient marine platform for solar panels. The concept may also be used to carry other relatively light-weight structures, or to support marine operations in sheltered areas that require a large, cost-efficient deck area.

ACKNOWLEDGEMENTS

We would like to acknowledge Prof. em. Bruce Patterson and Prof. em. Frode Mo for providing the presently investigated concept to the authors. We would like to thank Prof. Odd M. Faltinsen for useful suggestions and discussions during the present study.

REFERENCES

[1] O. M. Faltinsen. *Hydrodynamics of High-Speed Marine Vehicles*. Cambridge University Press, 2005.

[2] D. Kristiansen and O. M. Faltinsen. Non-linear wave-induced motions of cylindrical-shaped floaters of fish farms. *J. Engng. Maritime Env.*, 223:361–375, 2009.

[3] Trygve Kristiansen and Odd M. Faltinsen. Experimental and numerical study of an aquaculture net cage with floater in waves and current. *J. Fluids and Structures*, 54:1–26, April 2015.

[4] C. H. Lee and J. N. Newman. Wave effects on large floating structures with air cushions. *Marine Structures*, 13(4):315–330, July 2000.

[5] Nathan S. Lewis and Daniel G. Nocera. Powering the planet: Chemical challenges in solar energy utilization. *Proceedings of the National Academy of Sciences*, 103(43):15729–15735, October 2006.

[6] P. Li and O. M. Faltinsen. Wave-induced vertical response of an elastic circular collar of a floating fish farm. In *Int. Conf. on Hydrodynamics (ICHD), St. Petersburg, Russia*, 2012.

[7] Peng Li, Odd M. Faltinsen, and Claudio Lugni. Non-linear vertical accelerations of a floating torus in regular waves. *Journal of Fluids and Structures*, 66:589–608, October 2016.

[8] Š. Malenica, V. Nikola, and M. C. Young. Global hydroelastic model for liquid cargo ships. In *7th Int. Conf. on Hydroelasticity in Marine Technology*, Split, Croatia, 2015. F 0194.

[9] J. A Pinkster and E. J. A Meevers Scholte. The behaviour of a large air-supported MOB at sea. *Marine Structures*, 14(1):163–179, January 2001. F 0197.